IOPscience iopscience.iop.org

Home Search Collections Journals About Contact us My IOPscience

Focused ion-beam assisted deposition of tungsten and carbon

This article has been downloaded from IOPscience. Please scroll down to see the full text article.

1991 J. Phys.: Condens. Matter 3 S199

(http://iopscience.iop.org/0953-8984/3/S/032)

View the table of contents for this issue, or go to the journal homepage for more

Download details:
IP Address: 129.252.86.83
The article was downloaded on 27/05/2010 at 11:24

Please note that terms and conditions apply.

J. Phys.: Condens. Matter 3 (1991) S199–S206. Printed in the UK

Focused ion-beam assisted deposition of tungsten and carbon

D W K Jenkins†, G C Allen†, P D Prewett‡ and P J Heard§

† Interface Analysis Centre, University of Bristol, UK

‡ Rutherford Appleton Laboratory, Chilton, Oxford, UK

§ Oxford Instruments Ltd, Eynsham, Oxford, UK

Received 25 April 1991

Abstract. The process of ion-beam assisted deposition of tungsten and carbon by gallium ions has been studied using Auger electron spectroscopy (AES) and x-ray photoelectron spectroscopy (XPS). The bulk composition of tungsten and organic deposits was found to be 70/14/15/1 W/Ga/C/O and 64.4/34/1/0.6 C/Ga/O/Si at.% respectively. The deposition of tungsten results in the formation of a stable silicide complex at the interfacial region. The process of carbon deposition occurs by free radical formation and covalent bonding of organic molecules to the surface.

1. Introduction

The technique of focused ion-beam assisted deposition has gained much attention because it may facilitate the repair of integrated circuits [1, 2] and lithographic masks [3, 4]. Although electron and focused laser-beam induced chemical reactions have been used for the same purpose, ion-beam assisted deposition has the following desirable qualities: (i) the ability of the ion beam to be focused to a point of $<1\ \mu$m diameter with high resolution; (ii) high deposition rates; (iii) a vacuum of 10^{-6} to 10^{-7} mbar is required for operation; (iv) systems are commercially available, easy to use and compatible with other processes in the integrated circuit industry.

The mechanism of the ion-beam induced reactions is still not well understood. At the most basic level, molecules absorbed on the substrate are decomposed by the ion beam, resulting in the deposition of metal or carbon atoms on the surface. Some typical precursors used for deposition are listed in table 1. All these studies have used a focused gallium ion beam of between 20 and 50 keV to deposit the precursor material.

Table 1. Some precursors used in deposition.

Deposit	Precursor	Reference
Tungsten	Tungsten hexacarbonyl	[5]
	Tungsten hexafluoride	[4]
Gold	Dimethyl gold hexafluroacetyacetonate	[6, 7]
Tantalum	Pentaethoxy tantalum	[8]
Carbon	Styrene	[9]

0953-8984/91/SAS199 + 08 $03.50 © 1991 IOP Publishing Ltd

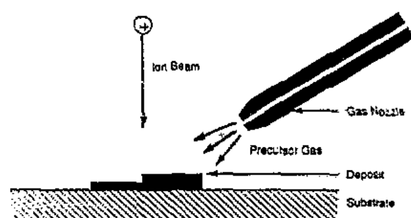

Figure 1. Precursor delivery system.

In this study the chemical bonding of the precursor to the substrate and the bulk composition of the deposited material has been examined by surface analytical techniques.

2. Experiment

The deposition experiments were carried out using the Oxford Instruments MicroTrim, at the Rutherford Appleton Laboratory, with a gallium ion beam of 42 keV and a range of beam fluxes between 6.25×10^{11} and 4.6×10^{14} ion cm^{-2}. Tungsten hexacarbonyl ($W(CO)_6$) and an oxygen-containing aromatic hydrocarbon were used to deposit tungsten and carbon respectively on a silicon surface at a pressure of 2×10^{-5} mbar. The gas delivery system used is illustrated in figure 1. $W(CO)_6$ was contained in an external reservoir heated to 40 °C. The aromatic hydrocarbon was introduced at room temperature. The precursors used were chosen for their general availability and stability at both atmospheric pressure and ambient temperature.

2.1. Auger electron spectroscopy (AES)

The tungsten deposits were analysed for tungsten, silicon, carbon, oxygen and gallium using a Perkin-Elmer PHI 595 scanning Auger electron spectrometer at the University of Bristol's Interface Analysis Centre. The carbon deposits were examined for carbon, silicon, oxygen and gallium. All spectra were recorded using a LaB_6 cathode operating at 5 kV. Depth profiling experiments were carried out using an Ar^+ ion source at 2 kV and a sample current of 3 μA. The etching rate was estimated to be 3 nm min^{-1}. Quantitative analysis of the Auger spectra obtained was carried out using relative Auger sensitivity factors [10].

2.2. X-ray photoelectron spectroscopy (XPS)

Areas of the surface measuring 200 μm^2 were analysed using a Kratos analytical axis small-area x-ray photoelectron spectrometer. Data were gathered in the binding energy range 0–1000 eV which included the photoelectron regions for the W 4f, Si 2p, C 1s and O 1s electron levels. All spectra were recorded using unmonochromatized Mg Kα radiation with the anode operating at 15 kV and 20 mA. Data handling and curve fitting were completed using DS800 software. Curve fitting of the spectra was carried out using a non-linear least-squares curve fitting program with a Gaussian product function.

3. Results

3.1. Tungsten deposits

3.1.1. Scanning electron microscopy (SEM) and Auger electron spectroscopy (AES) measurements. Decomposition of $W(CO_6)$ formed deposits of 5 μm^2 with ion-beam

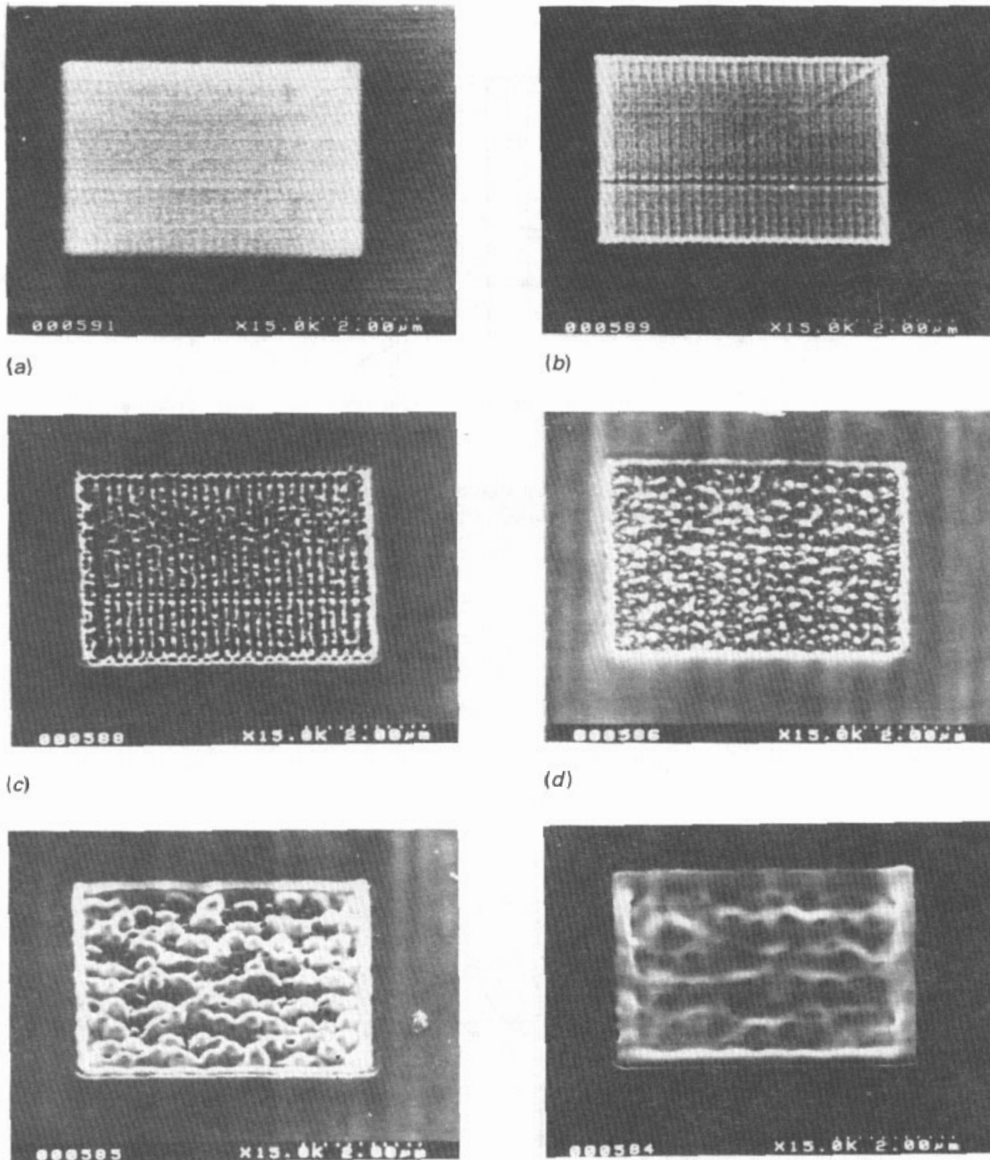

Figure 2. SEM images of tungsten deposits exposed to ion-beam fluxes (in ion cm^{-2}) of (*a*) 6.25×10^{11}; (*b*) 3.12×10^{12}; (c) 6.25×10^{12}; (*d*) 1.62×10^{13}; (*e*) 3.12×10^{13}; (*f*) 4.6×10^{13}.

fluxes of between 6.25×10^{11} and 4.6×10^{14} ion cm^{-2}. SEM and AES analyses were used to characterize the surface following the deposition experiments. Figures 2(*a*) to (*f*) show the changes of surface topography for tungsten deposits exposed to varying ion doses. Figure 2(*a*), resulting from the lowest ion flux used, shows a smooth surface primarily comprised of carbon. In figures 2(*b*) and (*c*), some removal of this preliminary carbon deposit is seen together with the subsequent deposition of tungsten along ion-beam raster lines. Figures 2(*d*) and (*e*) show sites of nucleation and subsequent infilling

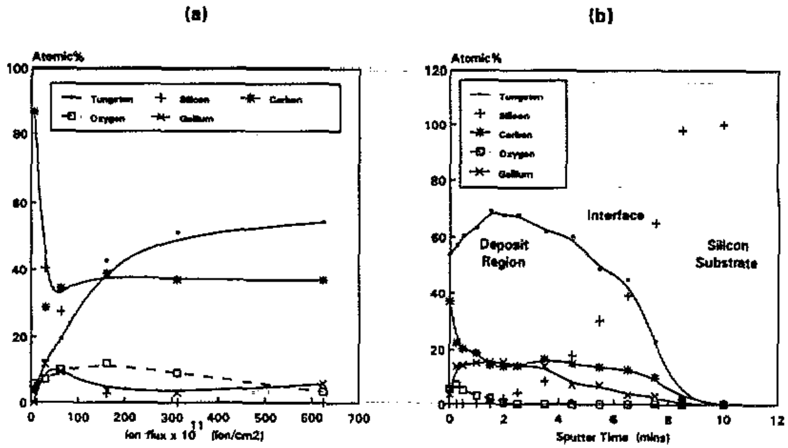

Figure 3. (*a*) Surface composition of tungsten deposits with varying ion flux. (*b*) Auger depth profile of tungsten deposit (produced by a ion flux of 4.6×10^{13} ion cm^{-2}).

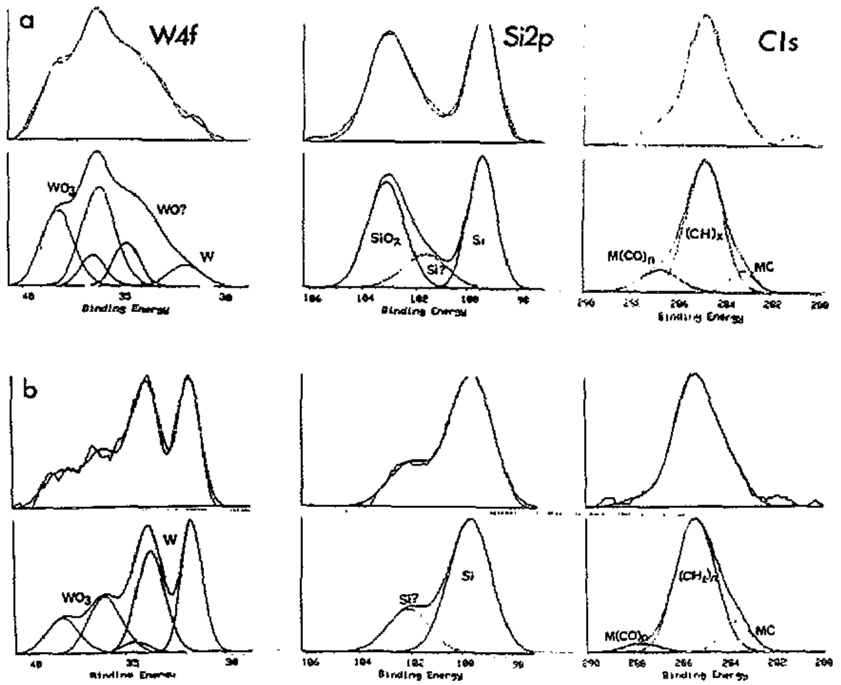

Figure 4. (*a*) W 4f, Si 2p and C 1s spectra of a tungsten deposit produced by a 6.25×10^{11} ion cm^{-2} ion-beam flux. (*b*) W 4f, Si 2p and C 1s spectra of a tungsten deposit produced by a 3.125×10^{13} ion cm^{-2} ion-beam flux.

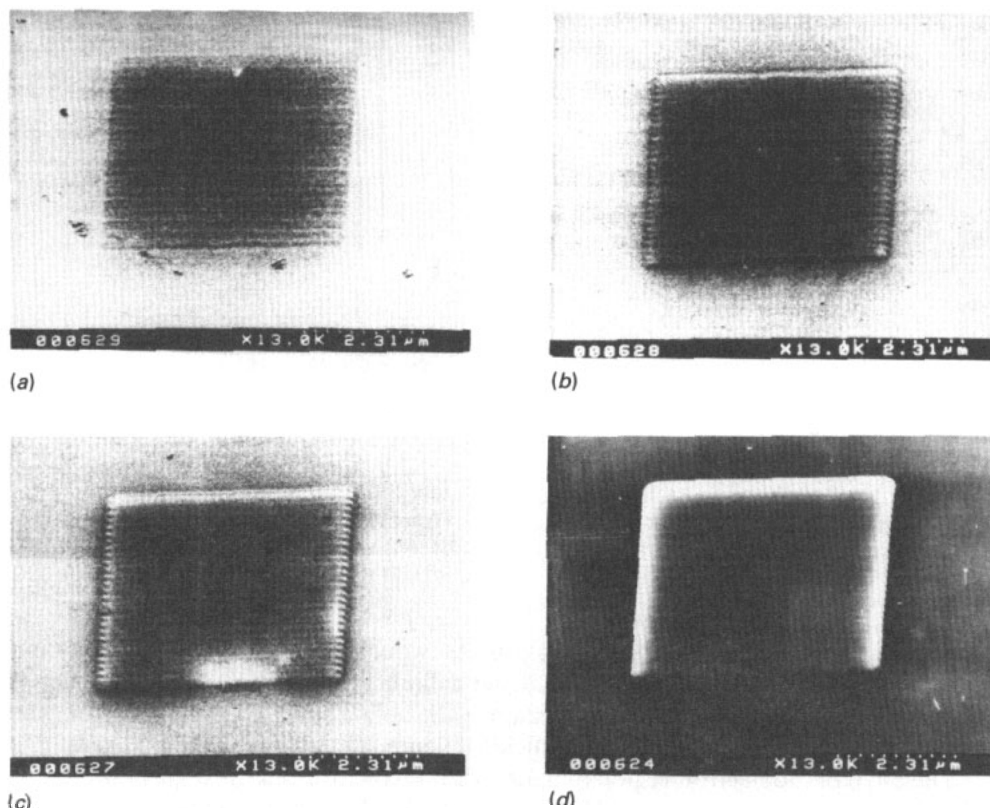

Figure 5. SEM images of tungsten deposits exposed to ion-beam fluxes (in ion cm^{-2}) of: (*a*) 6.25×10^{11}; (*b*) 3.12×10^{12}; (*c*) 1.62×10^{13}; and (*d*) 4.6×10^{13}.

of the tungsten deposit. In figure 2(*f*) infilling between nucleation sites can be seen to be almost complete, producing even film growth.

AES measurements from the surface of the deposits shown in figures 2(*a*) to (*f*), are displayed graphically in figure 3(*a*). These measurements were acquired prior to cleaning of the surface by argon ion etching. A depth profile of the thickest deposit formed with a gallium ion beam of 4.6×10^{14} ion cm^{-2} is illustrated in figure 3(*b*). After etching for 2 min the bulk composition in at.% was found to be W 70, C 15, O1 and Ga 14. Silicon was not detected in this film.

Gallium was found to be incorporated in all of the deposits, suggesting the implantation of this element from the depositing ion beam. Prewett and Heard have calculated the maximum depth distribution of implanted gallium to be between 0 and 10 nm under similar conditions [11].

3.1.2. XPS measurements. XPS measurements were recorded from a 200 μm^2 area of the freshly prepared deposits. Figures 4(*a*) and (*b*) show the change in the W 4f, Si 2p and C 1s photoelectron regions recorded from these surfaces which were prepared using different gallium ion fluxes. Figure 4(*a*) shows the surface analysis for the deposit formed with the low flux of 6.25×10^{11} ion cm^{-2}. Here the W 4f region is primarily associated with the metal oxides at a binding energy between 35 and 40 eV with very little evidence

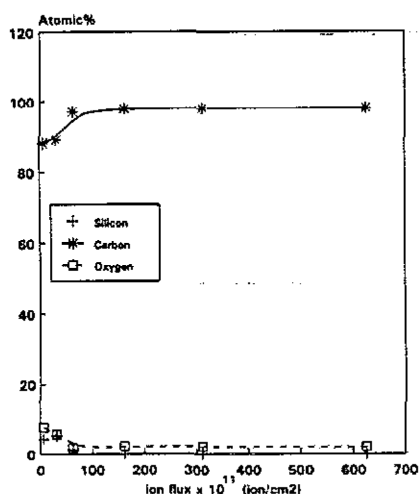

Figure 6. Surface composition of carbon deposits with varying ion flux.

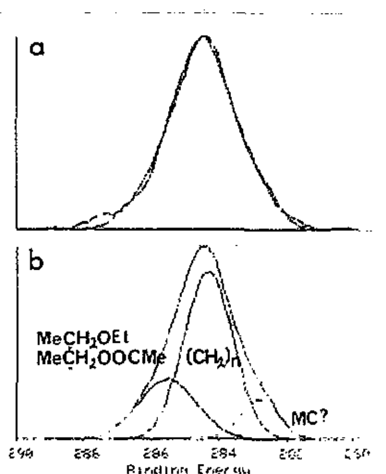

Figure 7. (*a*) C 1s spectra of carbon deposit produced by a 3.125×10^{13} ion cm^{-2} ion-beam flux. (*b*) C 1s spectra with curve fitting.

for metallic tungsten for which photoelectron lines would be expected to occur at binding energies between 30 and 35 eV. At the higher gallium ion flux of 3.12×10^{13} ion cm^{-2}, tungsten was observed in the metallic state, with only a small contribution from the tungsten oxides and possibly tungsten silicides (figure 4(*b*)).

The Si 2p photoelectron region in figure 4(*a*), recorded from the deposit produced using a low ion flux, clearly showed SiO_2, Si–Si and Si–W species, at binding energies of 103, 99, and 101 eV respectively [12]. At higher gallium-ion fluxes the Si 2p signal was found to be greatly reduced and SiO_2 was absent, leaving only elemental silicon and Si–W species. In both deposits carbon appeared to be present mainly as $(CH_2)_n$, although there was some evidence for small amounts of a carboxyl group at binding energy 287.5 eV and a carbide species at binding energy 283 eV [13].

3.2. Carbon deposits

3.2.1. SEM *and* AES *measurements.* SEM images of carbon deposits produced with different gallium-ion beam fluxes are shown in figures 5(*a*) to (*d*). Unlike the images obtained from the tungsten deposits produced under the same conditions, the topography was very smooth, indicating an even film growth. AES measurements on the deposit surfaces before depth profiling measurements using an argon-ion beam (see figure 6) clearly showing the formation of a film predominantly composed of carbon. It was also noted that gallium was absent from the surface of all these samples. After etching with an argon ion beam for 4 min, which removed an estimated 12 nm, the surface composition was found to be 68 at.% carbon and 32 at.% gallium on a atomic percentage basis. These values were subsequently confirmed by electron microprobe analysis which give values of 64.4% carbon, 34% gallium, 1% oxygen and 0.6% silicon.

3.2.2. XPS *measurements.* A typical x-ray photoelectron spectra from the C 1s region of a carbon deposit which had been produced using an ion flux of 3.12×10^{13} ion cm^{-2} is shown in figures 7(*a*) and (*b*). The broad carbon peak, figure 7(*a*), was considered to be

produced mainly by $(CH_2)_n$ species. The deconvolution of this peak as shown in figure 7(*b*) indicated the presence of other constituents. The high binding energy component could be attributed to >C=O species, whilst that at the lower binding energy is thought to arise from a Si–C bond.

4. Discussion

4.1. Tungsten deposition

The bulk deposit is primarily composed of tungsten in the form of tungsten metal, indicating that tungsten hexacarbonyl is completely decomposed during the deposition. From SEM and AES data, three stages of deposition are apparent, corresponding to:

(i) With a low gallium ion-beam flux a smooth deposit is formed consisting mainly of carbon. This probably arises form the ion-assisted deposition of organic contaminants in the system.

(ii) Higher ion-beam fluxes induce the removal of the carbon deposit and the natural substrate oxide layer by sputtering, thereby encouraging the nucleation of a tungsten deposit at the clean substrate surface along the direction of the rastered gallium ion beam.

(iii) With higher gallium ion fluxes, once the natural silicon oxide layer, of the substrate is completely removed deposition of tungsten occurs about the previously nucleated areas to produce a smooth surface.

For the thicker tungsten, AES depth profiling shows an interface region in which tungsten and silicon are present throughout a region of between 10 to 20 nm in thickness. At the interface of the deposit and substrate, a complex mixture of tungsten silicides is present. The most stable tungsten silicide is W_5Si_3 and it is probable that this compound is the most abundant in the interfacial region [14]. Such tungsten silicides are produced by solid state reactions at temperature of >650 °C, suggesting that the gallium ion beam must produce high temperatures at the surface of the substrate within the impact zone [15].

4.2. Carbon deposition

Under the same conditions used for the deposition of tungsten, carbon was observed by SEM images to be deposited at a greater rate. AES analysis indicated that the surface deposit consisted entirely of carbon. At a depth of approximately 12 nm, the composition of the bulk material were found in to be 68 at.% for carbon and 32 at.% for gallium. This is in relatively good agreement with the previous observation of Heard and Prewett [16] and suggests that gallium ions are absent from sites of recent deposition. This may be caused either by implantation of gallium to a greater depth than was seen in the tungsten deposits or by the continuation of carbon deposition after the termination of bombardment by the gallium ion beam.

The absence of an aromatic type carbon signal in the XPS spectrum recorded from the deposited material, suggests that the total decomposition of the aromatic ring has occurred and the low O/C ratio recorded implies the removal of oxygen from the compound.

The following bonding mechanism may be proposed for ion-assisted deposition of an oxygen containing aromatic hydrocarbon onto silicon. The cleavage of an Si–O bond

by a gallium ion, produces Si radical bonds which may bond with an incident vapour molecule. Bond formation with the substrate probably occurs via the vinyl or oxygen of the aromatic hydrocarbon, though the former may be favoured since bonding through the vinyl group would encourage delocalization of the unpaired electron, thereby stabilizing the resulting structure. Subsequent film formation may take several paths, but three processes must occur. These include the opening of the aromatic ring, together with crosslinking and subsequent removal of oxygen. The final carbon deposit takes a graphitic form although there is some evidence for the presence of carbonyl and carbide species as contaminants.

Gallium was found to be incorporated within the deposits investigated. Its presence appears to depend on the density of the layer under investigation. Thus, tungsten deposits contained approximately 15 at.% gallium, whilst carbon deposits were found to have incorporated 35 at.% gallium in the layers. This observation would be expected to be a consequence of several factors, including the decomposition of the vapour in the ion beam, the rate of removal of the surface through sputtering by the incident beam and the possible chemical interaction between the surface components and the implanted gallium. This element has for example been found in association with the C_2^- cluster on metal surfaces [17].

5. Conclusions

Ion-beam assisted deposition processes are similar for both organic and inorganic vapours. Both require the breakage and formation of chemical bonds. The deposition of tungsten, it is suggested, requires high surface temperatures for bonding to occur. This is likely to result in the formation at the interfacial region of a stable silicide complex of W_5Si_3. The process of carbon deposition probably occurs by free-radical formation and covalent bonding of organic molecules to the surface, leading to a faster deposition rate and rapid surface reconstruction.

References

[1] Stewart D K, Stern L A and Morgan J C 1989 *Proc. SPIE* **18** 1089
[2] Prewett P D 1991 unpublished
[3] Saitoh K Onoda H, Morimoto H, Watakabe T and Kato T 1988 *J. Vac. Sci. Technol.* B **6** 1032
[4] Gamo K and Namba S 1990 *Microelectron. Eng.* **11** 403
[5] Maskiko Y 1987 *25th Proc. Reliability Phys.* p 111
[6] Shedd G, Lezec H, Duber A D and Melngailis J 1986 *Appl. Phys. Lett.* **49** 1584
[7] Kirch S J and Wagner A 1990 *J. Vac. Sci. Technol.* A **8** 3705
[8] Gamo K 1986 *Microelectron. Eng.* **5** 2796
[9] Harriot L R and Vasile J 1989 *J. Vac. Sci. Technol.* B **7** 1954
[10] Davis L E, MacDonald N C, Palmberg P W, Riach G E and Weber R E (ed) 1978 *Handbook of Auger Electron Spectroscopy* (Minnesota: Physical Electronics Industries)
[11] Prewett P D and Heard P J 1987 *J. Phys. D: Appl. Phys.* **20** 1207
[12] Riviere J C 1983 *Technique and Application of X-ray Photoelectron Spectroscopy* AERE Harwell, R-10803 (London: HMSO)
[13] Wagen C D, Riggs W M, Davis L E, Moulder J F and Muilenberg G E (ed) 1979 *Handbook of X-ray Photoelectron Spectroscopy* (Minnesota: Physical Electronics Industries)
[14] Geib K M 1990 *J. Appl. Phys.* **68** 2796
[15] Chu J J 1987 *J. Appl. Phys.* **62** 465
[16] Heard P J and Prewett P D 1990 *Microelectron. Eng.* **11** 421
[17] Brown I T 1991 private communication